

# 6

## Debris-flow mechanics

*Richard M. Iverson*

### 6.1 INTRODUCTION

Debris flows involve gravity-driven motion of solid–fluid mixtures with abrupt surge fronts, free upper surfaces, variably erodible basal surfaces, and compositions that may change with position and time. These complications pose great challenges in efforts to understand debris-flow mechanics and predict debris-flow behavior. Recently, however, a combination of observational, experimental, and theoretical research has begun to yield a coherent picture of debris-flow mechanics. To help build a foundation for future research, this chapter emphasizes principles of debris-flow mechanics that are relatively well established and also highlights areas where critical knowledge is lacking. The chapter does not provide a comprehensive review of debris-flow mechanics literature, which has become voluminous during the past decade. An entree to this literature is provided by the proceedings of three International Conferences on Debris-Flow Hazards Mitigation: Mechanics, Prediction, and Assessment (Chen, 1997; Wieczorek and Naeser, 2000; Rickenmann and Chen, 2003).

### 6.2 MECHANICAL DEFINITION OF DEBRIS FLOW

Debris flows encompass a broad and imprecisely defined range of phenomena intermediate between dry rock avalanches and sediment-laden water floods, but to limit the scope of mechanical analysis, it is necessary to identify some distinguishing traits. Although debris flows are largely saturated with water, they differ from surging water floods in which sediment is held in suspension almost exclusively by fluid mechanical phenomena (e.g., viscous drag, buoyancy, turbulence). In such floods the presence of suspended sediment is mostly incidental to the dynamics of the flood wave as a whole. At the opposite extreme, although debris flows have sediment

concentrations comparable to those of rock avalanches, they differ from avalanches in which grains interact almost exclusively through solid-contact phenomena (e.g., collisions, adhesion, friction), perhaps mediated by intergranular air. In such avalanches the presence of water is mostly incidental to the dynamics of the avalanche as a whole. In contrast, strong interactions of the solid and liquid constituents are an essential element of the mechanics of debris flows. The magnitude and character of solid–liquid interactions may vary from flow to flow and within an individual flow, but the interactions always play a definitive mechanical role.

Typically, solid grains and intergranular liquid constitute roughly equal percentages (30–70%) of the volume of a debris flow. Rock avalanches can transform into debris flows through entrainment of water or water-rich sediment, and debris flows that entrain additional water can become so dilute that they transform to surging floods. Subaqueous debris flows can undergo a similar transformation as a result of entrainment of ambient water, thereby forming buoyancy-dominated gravity currents.

This chapter focuses on the mechanics of relatively simple subaerial debris flows in which average compositions remain more-or-less constant. Although the chapter emphasizes debris-flow motion, it presents a mechanical framework that also applies to quasistatic processes such as liquefaction during debris-flow initiation and consolidation of debris-flow deposits (cf. Iverson et al., 1997; Major and Iverson, 1999; Iverson et al., 2000; Iverson and Denlinger, 2001; Denlinger and Iverson, 2001). The conceptual continuity provided by this framework is important because debris-flow motion begins and ends in static states. In this respect debris flows have more in common with rock avalanches than with water floods.

### 6.3 MACROSCOPIC DYNAMICS

Any mechanical assessment of debris flows must begin with identification of the scale of behaviour of interest. This chapter adopts a continuum perspective, which considers behaviour on scales no smaller than that of representative elemental volumes (REVs) containing large numbers of individual solid grains (see Figure 6.1). The number of grains in an REV must be great enough that spatially and temporally averaged continuum quantities such as stress are meaningful and measurable, and are not subject to significant fluctuations due to the motion of individual grains. Drew and Lahey (1993) discuss mathematical issues regarding continuum averaging of fluctuating phenomena in grain–fluid mixtures. Iverson (1997) presents data that show how continuum stress fluctuations at the base of debris flows diminish as the size of the measurement device (or REV) increases to include the simultaneous effects of many thousands of grains.

An alternative approach to debris-flow mechanics considers behaviour at the scale of individual grains. Advances in computational power have facilitated progress in this area (e.g., Campbell et al., 1995; Asmar et al., 2003), but such a “discrete-body” approach appears unlikely to supplant continuum mechanics in the foreseeable future, as even laboratory-sized debris flows ( $\sim 10 \text{ m}^3$ ) commonly contain

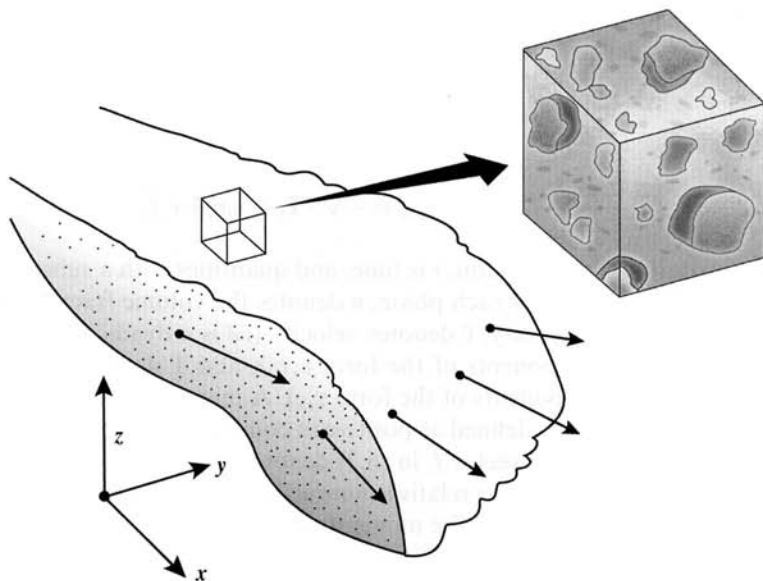


**Figure 6.1.** Definition of a REV containing a large number of solid grains as well as intergranular muddy fluid within a debris flow. Here the REV is a cube aligned with Cartesian coordinate axes, a geometry that is convenient but not essential.

more than  $10^{10}$  interacting grains (Iverson, 1997). Nevertheless, an intriguing possibility for the future involves melding continuum and discrete-body mechanics to investigate the interaction of isolated large clasts with adjacent, finer-grained debris (e.g., Yamagishi et al., 2003).

### 6.3.1 Continuum conservation laws

The conservation laws of classical physics provide the fundamental tools for analysis of debris-flow continuum mechanics. The most useful of these laws describe conservation of mass and linear momentum. Conservation of angular momentum also applies to debris flows, but in conventional continuum mechanics angular momentum is conserved implicitly through the use of a symmetric stress tensor, as is used here (e.g., Malvern, 1969). Conservation of energy applies to debris flows, but does not provide additional information if debris flows are treated as isothermal phenomena, as they are here (cf. Iverson, 1997). (In 1-D analyses of debris-flow motion, conservation of energy and linear momentum yield equivalent equations of motion because the vectorial character of momentum reduces to a scalar form like that of energy. However, this equivalence does not extend to multidimensional debris flows, wherein the vectorial character of momentum conservation makes it the most useful principle.)

Differential equations describing mass and linear momentum conservation, valid for each phase of a debris-flow mixture treated as a continuum, are (e.g., Gidaspow, 1994):

$$\frac{\partial \rho_i n_i}{\partial t} + \nabla \cdot \rho_i n_i \vec{v}_i = 0 \quad (6.1)$$

$$\frac{\partial \rho_i n_i \vec{v}_i}{\partial t} + \nabla \cdot \rho_i n_i \vec{v}_i \vec{v}_i = -\nabla \cdot \mathbf{T}_i + \rho_i n_i \vec{g} + \vec{f}_i \quad (6.2)$$

where  $\vec{g}$  is gravitational acceleration,  $t$  is time, and quantities with a subscript  $i$  apply to each phase individually. For each phase,  $n$  denotes the volume fraction (such that  $\sum n_i = 1$ ),  $\rho$  denotes mass density,  $\vec{v}$  denotes velocity ( $\vec{v}\vec{v}$  is a dyadic product: a  $3 \times 3$  tensor with Cartesian components of the form  $v_x v_y$ ), and  $\mathbf{T}$  denotes stress (a  $3 \times 3$  tensor with Cartesian components of the form  $\tau_{yx}$ ). A minus sign precedes the stress term in (6.2) because stress is defined as positive in compression, as is conventional in soil and rock mechanics. The vector  $\vec{f}_i$  in (6.2) denotes the interaction force per unit volume exerted on phase  $i$  due to relative motion of the other phase(s).

Terms on the left-hand side of the momentum-conservation equation (6.2) differ from those on the left-hand side of the mass-conservation equation (6.1) only through inclusion of an additional  $\vec{v}_i$ , reflecting the definition of momentum: mass times velocity. This connection between mass and momentum conservation is clear because (6.2) depicts the “conservative” form of the momentum equation. Some readers may be more familiar with the “primitive” momentum equation wherein, for example,  $\vec{v}_i \cdot \nabla \vec{v}_i$  replaces  $\nabla \cdot \vec{v}_i \vec{v}_i$  in (6.2). The primitive form is obtained by algebraic rearrangement of (6.2) and elimination of some terms through use of (6.1).

Conservation equations for the debris-flow mixture as a whole can be derived by summing the equations for the individual phases while using appropriately weighted averages to define the mixture density  $\rho = \rho_s n_s + \rho_f n_f$  and mixture velocity  $\vec{v} = (\rho_s n_s \vec{v}_s + \rho_f n_f \vec{v}_f) / \rho$ . Here subscripts  $s$  and  $f$  denote the solid and fluid phases indicated generically by “ $i$ ” in (6.1) and (6.2). Summation of (6.1) for the solid and fluid phases yields the mixture mass-conservation equation, which can be written in several alternative forms, including:

$$\frac{\partial \rho}{\partial t} + \nabla \cdot \rho \vec{v} = 0 \quad (6.3a)$$

$$\frac{1}{\rho} \frac{d\rho}{dt} + \nabla \cdot \vec{v} = 0 \quad (6.3b)$$

Similarly, summation of (6.2) for the solid and fluid phases yields the mixture momentum-conservation equation, which can be written in several forms including:

$$\frac{\partial \rho \vec{v}}{\partial t} + \nabla \cdot \rho \vec{v} \vec{v} = -\nabla \cdot \mathbf{T} + \rho \vec{g} \quad (6.4a)$$

$$\frac{d\vec{v}}{dt} = -\frac{1}{\rho} \nabla \cdot \mathbf{T} + \vec{g} \quad (6.4b)$$

In (6.3b) and (6.4b) the total time derivative  $d/dt$  represents the differential operator

$\partial/\partial t + \vec{v} \cdot \nabla$ , and it denotes differentiation in a frame of reference that moves with the mixture velocity  $\vec{v}$ . Derivatives of  $\rho$  do not appear in (6.4b) because they cancel from (6.4a) through subtraction of (6.3a). The interaction force  $\vec{f}_i$  in (6.2) does not appear explicitly in (6.4a) or (6.4b) because the force exerted on the solid grains by the fluid balances the force exerted on the fluid by the grains (thereby satisfying Newton's third law of motion).

Equations (6.3) and (6.4) are identical to the mass and momentum conservation equations for a single-phase continuous medium (cf. Malvern, 1969). However, the summed stress  $\mathbf{T}$  in (6.4) implicitly includes distinct contributions from solid and fluid phases and from relative motion of the phases (cf. Iverson, 1997; Iverson and Denlinger, 2001).

### 6.3.2 Depth integration and mass-change effects

A more useful form of the 3-D conservation equations (6.3) and (6.4) can be obtained by integrating the equations through the debris-flow thickness  $h$ , measured vertically from the bed at elevation  $z = b(x, y, t)$  to the flow surface at elevation  $z = \eta(x, y, t)$ , where  $x$  and  $y$  are planimetric coordinates (see Figure 6.2). Alternatively, depth integration can be performed in a direction normal to the bed, as presented, for example, by Savage and Hutter (1989, 1991), Iverson (1997), Gray et al. (1999), and Iverson and Denlinger (2001). Results are similar in either case, although vertical integration serves to highlight the influence of boundary conditions and non-hydrostatic stress states, which are elaborated below.

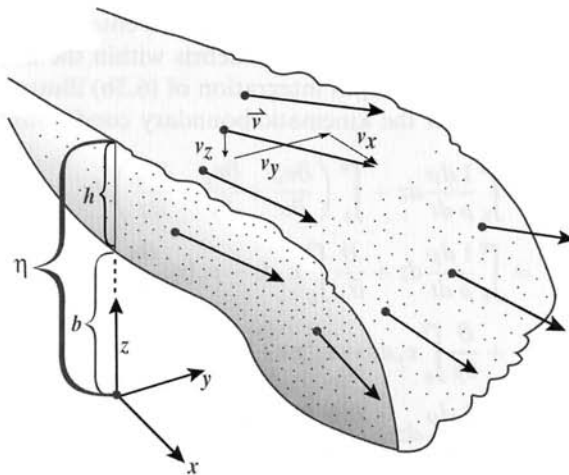


**Figure 6.2.** Definition of the Cartesian coordinate system, variable bed elevation  $b$ , variable debris thickness  $h = \eta - b$ , and variable velocity vectors in a depth-averaged debris-flow model obtained by vertical integration of the equations of motion. Cartesian velocity components ( $v_x$ ,  $v_y$ ,  $v_z$ ) are depicted for one of the velocity vectors, and  $v_z$  is negative when pointing downward as shown.

Prior to depth integration, the vector momentum equation (6.4) is disaggregated into component equations containing the  $x$ ,  $y$ , and  $z$  velocity components,  $v_x$ ,  $v_y$ , and  $v_z$  (see Figure 6.2). Integration of each component equation makes use of Leibniz' theorem for interchanging the order of integration and differentiation (Abramowitz and Stegun, 1964, p. 11). Most integrals are thereby absorbed into definitions of depth-averaged quantities such as the depth-averaged velocity components (denoted by overbars):

$$\bar{v}_x = \frac{1}{h} \int_{z=b}^{z=\eta} v_x dz \quad \bar{v}_y = \frac{1}{h} \int_{z=b}^{z=\eta} v_y dz \quad \bar{v}_z = \frac{1}{h} \int_{z=b}^{z=\eta} v_z dz \quad (6.5a, b, c)$$

Also absorbed into (6.3) and (6.4) during depth integration are kinematic boundary conditions, which specify volumetric fluxes of debris through the basal and upper surfaces of a debris flow due to erosion and sedimentation. The kinematic conditions may be written as:

$$v_z(\eta) = \frac{\partial \eta}{\partial t} + v_x(\eta) \frac{\partial \eta}{\partial x} + v_y(\eta) \frac{\partial \eta}{\partial y} + A(x, y, t) \quad (6.6)$$

$$v_z(b) = \frac{\partial b}{\partial t} + v_x(b) \frac{\partial b}{\partial x} + v_y(b) \frac{\partial b}{\partial y} + B(x, y, t) \quad (6.7)$$

In (6.6),  $A(x, y, t)$  specifies the rate of vertical accretion to a debris flow's surface as a result of collapse of adjacent bank material, for example. In (6.7),  $B(x, y, t)$  specifies the rate of bed elevation change as a result of sedimentation ( $B > 0$ ) or erosion ( $B < 0$ ). If no mass enters or leaves a debris flow,  $A$  and  $B$  as well as  $\partial b/\partial t$  equal zero. Depth integrations that embed the kinematic conditions (6.6 and 6.7) in the conservation equations (6.3 and 6.4) assume that debris entering or leaving the debris flow locally has the same bulk density as the debris within the flow.

The mathematical details of depth integration of (6.3b) illustrate use of Leibniz' theorem and incorporation of the kinematic boundary conditions (6.6) and (6.7):

$$\begin{aligned} \int_b^\eta \left( \frac{1}{\rho} \frac{d\rho}{dt} + \nabla \cdot \vec{v} \right) dz &= \int_b^\eta \frac{1}{\rho} \frac{d\rho}{dt} dz + \int_b^\eta \left( \frac{\partial v_x}{\partial x} + \frac{\partial v_y}{\partial y} + \frac{\partial v_z}{\partial z} \right) dz \\ &= \int_b^\eta \frac{1}{\rho} \frac{d\rho}{dt} dz + \frac{\partial}{\partial x} \int_b^\eta v_x dz - v_x(\eta) \frac{\partial \eta}{\partial x} + v_x(b) \frac{\partial b}{\partial x} \\ &\quad + \frac{\partial}{\partial y} \int_b^\eta v_y dz - v_y(\eta) \frac{\partial \eta}{\partial y} + v_y(b) \frac{\partial b}{\partial y} + v_z(\eta) - v_z(b) \\ &= \int_b^\eta \frac{1}{\rho} \frac{d\rho}{dt} dz + \frac{\partial(\bar{v}_x h)}{\partial x} + \frac{\partial(\bar{v}_y h)}{\partial y} \\ &\quad - \left[ v_x(\eta) \frac{\partial \eta}{\partial x} + v_y(\eta) \frac{\partial \eta}{\partial y} - v_z(\eta) \right] + \left[ v_x(b) \frac{\partial b}{\partial x} + v_y(b) \frac{\partial b}{\partial y} - v_z(b) \right] \\ &= \int_b^\eta \frac{1}{\rho} \frac{d\rho}{dt} dz + \frac{\partial(\bar{v}_x h)}{\partial x} + \frac{\partial(\bar{v}_y h)}{\partial y} + \frac{\partial h}{\partial t} + A - B = 0 \quad (6.8) \end{aligned}$$

The last line of (6.8) is obtained by substituting (6.6) and (6.7) into the fifth line of (6.8) and then using the substitution  $\partial\eta/\partial t - \partial b/\partial t = \partial h/\partial t$  (see Figure 6.2). If the debris bulk density  $\rho$  is constant, the integral in the last line of (6.8) vanishes, and the last line of (6.8) thereby reduces to the depth-integrated mass-conservation equation conventionally used in shallow-water theory (e.g., Vreugdenhil, 1994).

If  $\rho$  is not constant but the solid and fluid constituents of a debris flow are individually incompressible, the bulk density change  $d\rho/dt$  that appears in the integral in the last line of (6.8) can be expressed in terms of porosity change (i.e., fluid volume-fraction change), because  $d\rho/dt = (\rho_f - \rho_s)dn_f/dt$ . Changes in porosity imply relative motion of the solid and fluid constituents and thereby produce solid–fluid interaction stresses, as detailed below.

Mathematical operations similar to those in (6.8) are used to derive from (6.4) the depth-integrated momentum-conservation equations for the  $x$ ,  $y$ , and  $z$  directions:

$$\frac{\partial h\bar{v}_x}{\partial t} + \frac{\partial h\bar{v}_x^2}{\partial x} + \frac{\partial h\bar{v}_y\bar{v}_x}{\partial y} = -\frac{1}{\rho} \int_b^\eta \left[ \frac{\partial \tau_{xx}}{\partial x} + \frac{\partial \tau_{yx}}{\partial y} + \frac{\partial \tau_{zx}}{\partial z} \right] dz - Av_x(\eta) + Bv_x(b) \quad (6.9)$$

$$\frac{\partial h\bar{v}_y}{\partial t} + \frac{\partial h\bar{v}_y^2}{\partial y} + \frac{\partial h\bar{v}_x\bar{v}_y}{\partial x} = -\frac{1}{\rho} \int_b^\eta \left[ \frac{\partial \tau_{yy}}{\partial y} + \frac{\partial \tau_{xy}}{\partial x} + \frac{\partial \tau_{zy}}{\partial z} \right] dz - Av_y(\eta) + Bv_y(b) \quad (6.10)$$

$$\frac{\partial h\bar{v}_z}{\partial t} + \frac{\partial h\bar{v}_x\bar{v}_z}{\partial x} + \frac{\partial h\bar{v}_y\bar{v}_z}{\partial y} = -gh - \frac{1}{\rho} \int_b^\eta \left[ \frac{\partial \tau_{zz}}{\partial z} + \frac{\partial \tau_{xz}}{\partial x} + \frac{\partial \tau_{yz}}{\partial y} \right] dz - Av_z(\eta) + Bv_z(b) \quad (6.11)$$

Several features of these equations deserve emphasis. First, the equations apply even if the debris bulk density varies, provided that  $A$  and  $B$  represent boundary fluxes of debris with a bulk density equal to the local flow bulk density. Second, the gravitational forcing term  $-gh$  appears only in the  $z$  momentum equation (6.11), because gravity is assumed to act vertically downward. Motion in the  $x$  and  $y$  directions is driven by stress gradients that arise in reaction to this gravitational forcing. Third, the non-linear advective acceleration terms (which contain velocity products such as  $\bar{v}_x^2$  and  $\bar{v}_y\bar{v}_x$ ) neglect the effects of non-uniform vertical velocity profiles, which produce differential advection of momentum (cf. Vreugdenhil, 1994). Compensation for this neglect involves adding momentum “correction coefficients” to the advective acceleration terms. However, such coefficients are omitted here because vertical velocity profiles in debris flows are poorly constrained and are likely variable (Iverson and Vallance, 2001). Therefore, at this juncture, addition of momentum correction coefficients to the momentum-conservation equations would add no mechanical insight.

The presence of the erosion and sedimentation terms involving  $A$  and  $B$  on the right-hand side of (6.9), (6.10), and (6.11) distinguishes these equations from typical depth-integrated momentum equations, such as those of Denlinger and Iverson (2004). Mathematically, these terms arise from use of (6.6) and (6.7) during depth integration. Physically, these terms represent the momentum change associated with

accelerating newly added mass (assumed to have no initial velocity) to the speed of the debris flow or with expelling debris-flow mass to create a static deposit. The terms are exact insofar as mathematical book-keeping is concerned, but they do not account fully for the mechanics of the erosion or deposition processes. Erlichson (1991) likened mass-change terms such as those in (6.9), (6.10), and (6.11) to mass-change terms in rocket equations: only in systems in which mass change occurs independently of external forces do such terms account completely for momentum change produced by mass change. Otherwise, it is necessary to account explicitly for the external forces that *cause* the mass change, as well as for the *effects* of mass change as represented in (6.9), (6.10), and (6.11).

Conservation equations such as (6.9), (6.10), and (6.11) provide a starting point for investigation of erosion and sedimentation by debris flows, but characterization of forces that cause such mass change remains largely speculative and requires further research. For this reason, and to streamline the mathematics in the remainder of this chapter, the assumption  $A = B = 0$  will be used hereafter.

### 6.3.3 Scaling and shallow flow with non-hydrostatic stress

Virtually all computational models of debris-flow motion use some form of shallow-flow approximation. Shallow-flow approximations of 4-D conservation laws (involving three space coordinates plus time, as in (6.8)–(6.11)) reduce the number of governing equations and dependent variables from 4 to 3, thereby facilitating computation of solutions (e.g., Denlinger and Iverson, 2001). Shallow-flow approximations also simplify evaluation of stresses – a particularly significant advantage when stress states are poorly constrained (e.g., Iverson and Denlinger, 2001). Below, scaling of (6.8)–(6.11) is used to obtain a shallow debris-flow approximation that is valid on both steep and gentle slopes. This approximation subsumes as a special case the approximation commonly used in shallow-water theory (cf. Vreugdenhil, 1994).

For either debris flows or shallow-water flows of finite extent, the pertinent length scale in the  $z$  direction is the typical flow thickness  $H$ , whereas the length scale in the  $x$  and  $y$  directions is a typical planimetric dimension (length, width) of the flow  $L$  (Figure 6.3). Velocity components in the  $x$ ,  $y$ , and  $z$  directions scale with the product of gravitational acceleration and the pertinent length scale ( $L$  or  $H$ ) raised to the  $\frac{1}{2}$  power, and time scales with  $(L/g)^{1/2}$  because gravity drives time-dependent motion dominantly in the  $x$  and  $y$  directions. All stress components in (6.9), (6.10), and (6.11) scale with the static stress due to gravity,  $\rho g H$ , because gravity and its effect on debris weight are the fundamental phenomena driving motion. These scalings are summarized by (cf. Savage and Hutter, 1989):

$$x, y \sim L \quad z \sim H \quad (6.12a, b)$$

$$\tau_{xx}, \tau_{yy}, \tau_{zz}, \tau_{yx}, \tau_{zx}, \tau_{yz} \sim \rho g H \quad (6.12c)$$

$$\bar{v}_x, \bar{v}_y \sim (gL)^{1/2} \quad \bar{v}_z \sim (gH)^{1/2} \quad t \sim (L/g)^{1/2} \quad (6.12d, e, f)$$

Typically  $H/L \ll 1$  because debris flows generally have more-or-less tabular geometries like that shown in Figure 6.3. As a consequence of this geometry and

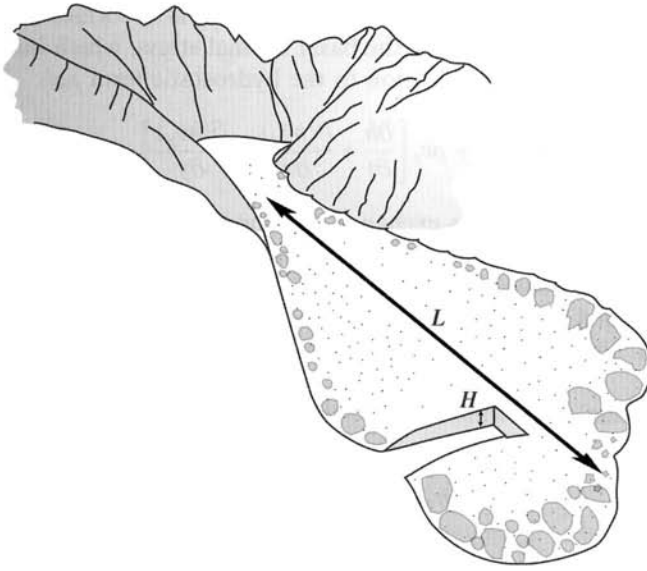


**Figure 6.3.** Schematic of typical, tabular debris-flow geometry, illustrating the length scales  $H$  and  $L$ .

the scalings in (6.12a, b, c, d, e, f), the stress derivatives with respect to  $x$  and  $y$  in (6.9), (6.10), and (6.11) are inferred to be significantly smaller than the stress derivatives with respect to  $z$  (by a factor  $\sim H/L$ ). Similarly, the velocity component in the  $z$  direction is inferred to be smaller than the velocity components in the  $x$  and  $y$  directions (by a factor  $\sim (H/L)^{1/2}$ ). Thus, a rational approximation of the vertical momentum equation (6.11) can be obtained by omitting the relatively small terms involving  $z$  velocity components and  $x$  and  $y$  derivatives of stress components. Omission of these terms reduces (6.11) to a simple hydrostatic stress balance  $\int_b^\eta (\partial \tau_{zz} / \partial z) dz = -\rho gh$ , and integration of this equation using the free-surface boundary condition  $\tau_{zz}(\eta) = 0$  yields a hydrostatic basal normal stress  $\tau_{zz}(b) = \rho gh$ . This is the stress state (and supporting rationale) assumed in conventional shallow-water theory (e.g., Vreugdenhil, 1994).

In debris flows the stress state may differ significantly from the hydrostatic state assumed in conventional shallow-water theory, in part because vertical accelerations (involving  $\bar{v}_z$ ) may not be negligible. Vertical accelerations effectively change the weight of a moving debris mass, and their consequent effect on stresses is apt to be particularly important where debris flows encounter steep slopes or irregular terrain that deflects the flow. If vertical accelerations are significant, a suitable approximation of the vertical momentum equation (6.11) can be obtained by neglecting the terms involving  $x$  and  $y$  derivatives of stress (of order  $H/L$ ) but retaining the vertical velocity terms (of order  $(H/L)^{1/2}$ ), yielding:

$$\frac{\partial(h\bar{v}_z)}{\partial t} + \frac{\partial(h\bar{v}_x\bar{v}_z)}{\partial x} + \frac{\partial(h\bar{v}_y\bar{v}_z)}{\partial y} = -\frac{1}{\rho} \int_b^\eta \frac{\partial \tau_{zz}}{\partial z} dz - gh \quad (6.13)$$

Evaluating the integral in (6.13) and inferring that the flow surface is stress-free (i.e.,  $\tau_{zz}(\eta) = 0$ ) yields an expression for the basal normal stress, which includes dynamic terms due to  $z$  momentum in addition to the hydrostatic term  $\rho gh$ :

$$\tau_{zz}(b) = \rho gh + \rho \bar{v}_z \left[ \frac{\partial h}{\partial t} + \frac{\partial(h\bar{v}_x)}{\partial x} + \frac{\partial(h\bar{v}_y)}{\partial y} \right] + \rho h \frac{d\bar{v}_z}{dt} \quad (6.14)$$

For debris flows with no mass exchange with boundaries ( $A = B = 0$ ), (6.14) simplifies because the terms in brackets reduce to a single term through application of the depth-averaged mass-conservation equation (6.8). (Note that when  $d/dt$  operates on a depth-averaged quantity, such as  $\bar{v}_z$  in (6.14), it represents a total time derivative advected with the depth-averaged horizontal motion,  $d/dt = \partial/\partial t + \bar{v}_x \partial/\partial x + \bar{v}_y \partial/\partial y$ .)

After applying (6.8) with  $A = B = 0$  to the terms in brackets (6.14) can be rewritten as:

$$\tau_{zz}(b) = \rho g' h - \rho \bar{v}_z \int_b^\eta \frac{1}{\rho} \frac{d\rho}{dt} dz \quad (6.15)$$

where  $g'$  denotes a total vertical acceleration defined by:

$$g' = g + \frac{d\bar{v}_z}{dt} \quad (6.16)$$

Equation (6.15) constitutes the central approximation in a shallow-flow theory for motion of debris flows on steep, irregular slopes, and it reduces to the hydrostatic approximation if  $d\bar{v}_z/dt = 0$  and  $d\rho/dt = 0$ . For debris flows in which  $\rho$  is nearly constant, the magnitude of the term containing  $g'$  in (6.15) greatly exceeds the magnitude of the term containing  $d\rho/dt$ , and the integral in (6.15) can be neglected. Ramifications of (6.15) and (6.16) for evaluation of stress components in addition to  $\tau_{zz}$  are discussed below.

For (6.15) and (6.16) to be useful, estimation of  $\bar{v}_z$  is necessary. A suitable estimate results from approximating the value of  $\bar{v}_z$  with the mean of the surface and basal values of  $v_z$ , which is obtained by inserting the depth-averaged velocity components  $\bar{v}_x$  and  $\bar{v}_y$  in the kinematic boundary conditions (6.6) and (6.7):

$$\bar{v}_z \approx \frac{1}{2} \left[ \frac{\partial \eta}{\partial t} + \bar{v}_x \frac{\partial \eta}{\partial x} + \bar{v}_y \frac{\partial \eta}{\partial y} \right] + \frac{1}{2} \left[ \frac{\partial b}{\partial t} + \bar{v}_x \frac{\partial b}{\partial x} + \bar{v}_y \frac{\partial b}{\partial y} \right] \quad (6.17)$$

Through use of (6.15), (6.16), and (6.17), effects of vertical accelerations can be included in stress evaluations without including  $\bar{v}_z$  as an explicit dependent variable (Denlinger and Iverson, 2004).

An alternative way of representing the effects of vertical accelerations on stresses involves use of curvilinear coordinate systems fitted to topography. In this case, vertical accelerations are represented by the combined effects of downslope accelerations and centripetal accelerations that are induced as flows traverse the topography (cf. Savage and Hutter, 1991; Hungr, 1995; Gray et al., 1999; Iverson and Denlinger, 2001). However, such an approach is difficult to implement if topographic

curvature has both  $x$  and  $y$  components and topography is as irregular as that of most natural debris-flow paths.

## 6.4 STRESS ESTIMATION

Whereas development of applicable conservation equations for shallow debris flows (i.e., equations 6.8, 6.9, 6.10, and 6.15) is tightly constrained by universal physical laws, mathematical rules, and scaling principles, stress estimation is more ambiguous. Stresses are important because they do the irreversible small-scale work that is responsible for continuum-scale energy dissipation and resistance to debris-flow motion. Of course, stress is simply a surrogate for the effects of momentum transport at scales too small to be resolved at a continuum scale. Therefore, momentum transport at scales much smaller than that of a continuum REV (Figure 6.1) can in principle be analysed to gain insight about stress and rheology, which relates stress to deformation. However, this chapter focuses on the continuum viewpoint and depth-averaged modeling described above, and does not present such analyses.

An advantage of depth-averaged debris-flow modeling is that the magnitude of one crucial stress component can be estimated without ambiguity:  $\tau_{zz}(b)$  is given by (6.15) regardless of flow rheology. Estimation of the magnitudes of other individual stress components depends on rheology but can be simplified by first applying Leibniz' theorem to the integrals on the right-hand sides of (6.9) and (6.10). From (6.9) this operation yields:

$$\int_b^\eta \left[ \frac{\partial \tau_{xx}}{\partial x} + \frac{\partial \tau_{yx}}{\partial y} + \frac{\partial \tau_{zx}}{\partial z} \right] dz = \frac{\partial \bar{\tau}_{xx} h}{\partial x} + \tau_{xx}(b) \frac{\partial b}{\partial x} + \frac{\partial \bar{\tau}_{yx} h}{\partial y} + \tau_{yx}(b) \frac{\partial b}{\partial y} - \tau_{zx}(b) \quad (6.18)$$

and an exactly analogous expression arises from (6.10). When Leibniz' theorem is used to obtain (6.18), some terms vanish because the upper surface of the flow (at  $z = \eta$ ) is assumed free of all stresses. Stress components with overbars in (6.18) denote depth-averaged quantities defined by integrals analogous to those in (6.5).

Terms on the right-hand side of (6.18) can be grouped into two categories. The collection of terms  $-\tau_{zx}(b) + \tau_{xx}(b)[\partial b/\partial x] + \tau_{yx}(b)[\partial b/\partial y]$  describes basal resistance to motion, and includes both a shear stress term  $\tau_{zx}(b)$  and two "form drag" terms that are non-zero if the local components of bed slope ( $\partial b/\partial x$ ,  $\partial b/\partial y$ ) result in a component of horizontal force directed into or out of the bed. These form drag terms vanish if depth integration is performed normal to the bed, rather than vertically, as is performed above (cf. Iverson and Denlinger, 2001). However, if the bed topography is irregular, depth integration normal to the bed results in spatial variation of the integration direction, which leads to other mathematical complications (Keller, 2003).

Additional terms on the right-hand side of (6.18),  $\partial(\bar{\tau}_{xx} h)/\partial x + \partial(\bar{\tau}_{yx} h)/\partial y$ , express the influence of depth-averaged horizontal stress gradients. These terms are non-zero even in steady, uniform flows on slopes, because the flow depth at a fixed  $z$  varies as a function of  $x$  and  $y$  in such flows. If depth integration is performed

normal to the bed, the terms  $\partial(\bar{\tau}_{xx}h)/\partial x + \partial(\bar{\tau}_{yx}h)/\partial y$  have the same form as in (6.18), but the terms vanish if flow is steady and uniform.

A lowest order approximation of the stress terms on the right-hand side of (6.18) can be identified by using the scalings summarized in (6.12). The scalings indicate that the basal resistance is of the order of  $\rho g H$ , whereas the terms involving the depth-averaged horizontal stresses  $\bar{\tau}_{xx}$  and  $\bar{\tau}_{yx}$  are smaller, of the order of  $\rho g H^2/L$  (where  $H/L \ll 1$ ). Thus, basal shear resistance has primary importance in depth-averaged debris-flow models, although the effects of lateral stress gradients cannot be ignored when modeling surge-like motion (Savage and Hutter, 1989).

### 6.4.1 Stress partitioning

As noted above, stresses in debris flows include distinct contributions from solid grains, intergranular fluid, and solid–fluid interactions. This partitioning of stress motivates two fundamental questions: In a debris mixture comprising a great diversity of grains and fluids, how are the solid and fluid phases distinguished? Once a distinction between solids and fluids is made, how is partitioning of stress determined?

Definition of the fluid phase in debris flows is not as simple as it might seem. The most straightforward definition (that the fluid consists of pure liquid water and pure gaseous air) is not the most useful for analysing debris-flow mechanics. To a large degree, air can be excluded from consideration because its low density, its low viscosity, and its large compressibility make its mechanical effects very small compared to those of liquid water. Furthermore, liquid water in debris flows generally carries small solid grains that can remain suspended solely as a consequence of buoyancy, viscosity, and turbulence. Because suspension of these small grains can occur in the absence of direct grain-to-grain contacts, it is not appropriate to treat the suspended grains as solids that transfer momentum only through direct contacts. Therefore, the discussion below defines the fluid phase of debris flows as water plus suspended small grains, which can in turn influence the effective fluid properties.

A scaling criterion can be used to distinguish the sizes of grains that are treated as part of the debris-flow fluid (Iverson, 1997). If the duration  $t_D$  of a debris flow is long in comparison with the time required for settling of a grain in static, pure water, the grain must be considered part of the solid fraction. On the other hand, if a grain can remain suspended for times that exceed  $t_D$  as a result of only water viscosity and buoyancy, the grain acts as part of the fluid. Durations of debris flows range from about  $t_D = 10$  s for small but significant events to  $10^4$  s for the largest. The time scale for grain settling (in the absence of other grains) can be estimated by dividing the characteristic settling distance or half thickness of a debris flow  $H/2$  by the grain settling velocity  $v_{set}$  estimated from Stokes law or a more general equation that accounts for grain inertia (Vanoni, 1975). Thus if  $H/(2t_D v_{set}) < 1$  the debris-flow duration is large compared with the time scale for grain settling. The half thickness of debris flows ranges from about 0.01 m for small flows to 10 m for large ones. Thus  $H/(2t_D) \sim 0.001$  m/s is typical for both small and large debris flows, which implies

that  $v_{set} < 0.001$  m/s is required for grains to act as part of the fluid. In water, grain settling velocities of  $\sim 0.001$  m/s or less occur if grain diameters are less than about 0.05 mm (Vanoni, 1975). This critical grain size corresponds reasonably well with the conventional silt–sand boundary (0.0625 mm), and it also falls in the range where settling is characterized by grain Reynolds numbers much smaller than 1, such that viscous and buoyancy forces dominate grain motion. By this rationale, a useful but inexact guideline states that grains larger than silt-size generally constitute the solid phase in debris flows, whereas grains in the silt–clay (i.e., “mud”) size fraction act as part of the fluid. Size distributions of grains in muddy fluids drained from freshly emplaced debris-flow deposits support this interpretation (Iverson, 1997).

Stress partitioning between the solid and fluid phases in mixtures can be accomplished in a variety of ways, but for debris flows it is convenient to employ a partitioning that is consistent with well-established conventions of soil mechanics (cf. Passman and McTigue, 1986). Thus, the total mixture stress  $T$  can be partitioned as (cf. Iverson, 1997; Iverson and Denlinger, 2001):

$$T = T_e + Ip + nT_{vis} \quad (6.19)$$

where  $T_e$  is the effective stress,  $p$  is the pore-fluid pressure,  $I$  is the identity tensor (which in equation 6.19 indicates that fluid pressure acts isotropically),  $T_{vis}$  is the viscous or deviatoric fluid stress (total fluid stress minus pressure), and  $n$  is the mixture porosity (or fluid volume fraction). This stress partitioning treats  $T_e$  and  $p$  as stresses that effectively act throughout the mixture (just as in conventional soil mechanics), whereas  $T_{vis}$  acts only within the fluid phase. For the special case in which the fluid is essentially static and the state of stress is 1-D (6.19) reduces to the familiar effective-stress definition of Terzaghi (1936):

$$\sigma = \sigma_e + p \quad (6.20)$$

where  $\sigma$  denotes a normal-stress component and  $\sigma_e$  is effective normal stress. However, definitions such as (6.19) and (6.20) imply nothing about the mechanical roles of pore pressure or effective stress; they merely provide a convenient means of partitioning the total stress.

#### 6.4.2 Stress due to solid–fluid interaction

Practical application of (6.19) and (6.20) requires specification of the mechanical roles of pore-fluid pressure and effective stress in debris flows. Clearly, these roles may be very complicated, because solid and fluid constituents in grain–fluid mixtures may interact in diverse ways (Iverson, 1997; Koch and Hill, 2001). However, to provide the simplest viable theory and establish a link with classical soil mechanics, the analysis below employs three postulates about the bulk interactions of solids and fluids in continuum REVs like that shown in Figure 6.1: the fluid pressure  $p$  mediates solid–fluid interactions; a linear drag equation specifies how fluid pressure gradients are coupled to relative motion of solid grains and intergranular fluid; and effective stress governs solid-contact friction. As shown below, use of these postulates in conjunction with mass conservation laws yields a theoretical

framework that can be applied to rapid flows with large deformations as well as to the special cases of quasistatic liquefaction and consolidation of soils.

For a debris-flow mixture with porosity  $n$  fully saturated with liquid, the mass-conservation equations for the fluid and solid phases can be inferred directly from (6.1). The equations are:

$$\frac{\partial[n\rho_f]}{\partial t} + \nabla \cdot [\vec{v}_f n \rho_f] = 0 \quad (6.21)$$

$$\frac{\partial[(1-n)\rho_s]}{\partial t} + \nabla \cdot [\vec{v}_s(1-n)\rho_s] = 0 \quad (6.22)$$

where subscripts  $f$  and  $s$  denote the fluid and solid phases, respectively. If the densities of the solid and fluid phases are constant (a reasonable assumption for the stress magnitudes  $< 100$  kPa typical of debris flows) then (6.21) and (6.22) reduce to:

$$\partial n / \partial t + \nabla \cdot (\vec{v}_f n) = 0 \quad (6.23)$$

$$-\partial n / \partial t - \nabla \cdot (n \vec{v}_s) + \nabla \cdot \vec{v}_s = 0 \quad (6.24)$$

Addition of (6.23) and (6.24) yields a special form of the mixture mass-conservation equation, which shows how the divergence of solid grain velocities  $\nabla \cdot \vec{v}_s$  must be balanced by flow of fluid relative to the grains:

$$\nabla \cdot \vec{v}_s = -\nabla \cdot n(\vec{v}_f - \vec{v}_s) \quad (6.25)$$

An additional equation shows how the same divergence must be balanced by changes in porosity. The equation is obtained by rearranging (6.24) as:

$$\nabla \cdot \vec{v}_s = \frac{\partial n}{\partial t} + \nabla \cdot (n \vec{v}_s) = \frac{d_s n}{dt} + n(\nabla \cdot \vec{v}_s) = \frac{1}{1-n} \frac{d_s n}{dt} \quad (6.26)$$

where  $d_s/dt = \partial/\partial t + \vec{v}_s \cdot \nabla$  denotes a total time derivative in a frame of reference advected with the velocity of the solid grains  $\vec{v}_s$ . Equating (6.25) and (6.26) yields a particularly useful form of the mixture mass-conservation equation (6.3b), which is exact if the solid and fluid phases are individually incompressible:

$$\frac{d_s n}{dt} = -(1-n)\nabla \cdot n(\vec{v}_f - \vec{v}_s) \quad (6.27)$$

This equation shows that local porosity changes necessarily are accompanied by differences in the local solid and fluid velocities. Even slight velocity differences have large mechanical ramifications if they result in significant solid–fluid drag.

Equation (6.27) can be converted to a form that uses a total time derivative advected with the mean mixture velocity,  $d/dt = \partial/\partial t + \vec{v} \cdot \nabla$ . This conversion is important because  $d/dt$  is the total time derivative used in (6.3b) and (6.4b) to describe mixture mass and momentum change, and it is helpful to express porosity change in the same frame of reference. Some simple algebraic substitutions and cancellations show that:

$$\frac{dn}{dt} - \frac{d_s n}{dt} = \left( \frac{\rho_s[1-n]}{\rho} - 1 \right) \vec{v}_s \cdot \nabla n + \left( \frac{\rho_f n}{\rho} \right) \vec{v}_f \cdot \nabla n = \frac{\rho_f n}{\rho} (\vec{v}_f - \vec{v}_s) \cdot \nabla n \quad (6.28)$$

Therefore, by utilizing (6.28), (6.27) can be rewritten as:

$$\frac{dn}{dt} = -(1-n)\nabla \cdot n(\vec{v}_f - \vec{v}_s) + \frac{\rho_f n}{\rho} (\vec{v}_f - \vec{v}_s) \cdot \nabla n \quad (6.29)$$

The solid–fluid velocity difference  $\vec{v}_f - \vec{v}_s$  that appears in (6.27), (6.28), and (6.29) implies the existence of drag due to relative motion of solid grains and adjacent fluid. A simple estimate of this drag for continuum REV's (Figure 6.1) assumes that it is proportional to the gradient in excess fluid pressure  $p_e$  that arises in reaction to relative motion of grains and fluid (where  $p_e$  is defined as total fluid pressure minus hydrostatic fluid pressure). This reasoning yields a linear drag equation with the same form as Darcy's law, which may be written as:

$$\vec{v}_f - \vec{v}_s = \frac{\vec{q}}{n} = -\frac{k}{n\mu} \nabla p_e \quad (6.30)$$

Here  $\vec{q}$  is the specific discharge of fluid (the flux relative to the adjacent granular aggregate),  $k$  is the intrinsic hydraulic permeability of the granular aggregate,  $\mu$  is the fluid viscosity, and the coefficient group  $k/n\mu$  may be viewed as a drag parameter. Bear (1972) provides an intensive discussion of Darcy's law and its interpretation for quasistatic rocks and soils. Experimental data indicate that Darcian drag is probably prevalent even in liquefied debris-flow mixtures (Iverson, 1997; Major et al., 1997).

Substitution of (6.30) into (6.27) and (6.29) yields alternative forms of an equation describing diffusive redistribution of excess pore pressure that occurs in response to porosity change:

$$\frac{1}{1-n} \frac{d_s n}{dt} = \nabla \cdot \frac{k}{\mu} \nabla p_e \quad (6.31a)$$

$$\frac{dn}{dt} = \left[ (1-n)\nabla - \frac{\rho_f}{\rho} \nabla n \right] \cdot \frac{k}{\mu} \nabla p_e \quad (6.31b)$$

Slight changes in porosity  $n$  can produce very significant changes in excess pore pressure  $p_e$  because plausible values of the coefficient  $k/\mu$  in (6.31a, b) range from about  $10^{-16}$  to  $10^{-6} \text{ m}^3 \text{ kg}^{-1} \text{ s}$  for debris-flow mixtures (Iverson, 1997; Major et al., 1997).

A more familiar form of the excess pore-diffusion equation arises from defining a debris bulk compressibility  $\alpha$  such that:

$$\frac{1}{1-n} \frac{d_s n}{dt} = -\alpha \frac{d_s \bar{T}_e}{dt} \quad (6.32)$$

where  $\bar{T}_e$  is the mean effective normal stress (*cf.* Savage and Iverson, 2003). Substitution of (6.32) in (6.31a) yields an equation that shows how excess pore pressure changes in response to changes in effective stress:

$$\frac{d_s \bar{T}_e}{dt} = -\frac{1}{\alpha} \nabla \cdot \left( \frac{k}{\mu} \nabla p_e \right) \quad (6.33)$$

Alternatively, the definition of effective stress (equation 6.19) can be used to rewrite (6.33) as a forced diffusion equation for excess pore pressure  $p_e$ :

$$\frac{d_s p_e}{dt} = \frac{1}{\alpha} \nabla \cdot \left( \frac{k}{\mu} \nabla p_e \right) + \frac{d_s}{dt} [\bar{T} - \rho_f g(\eta - z)] \quad (6.34)$$

where  $\rho_f g(\eta - z)$  is the hydrostatic component of pore pressure.

Several attributes of (6.34) are noteworthy. Equation (6.34) is similar to pore-pressure diffusion equations used in standard theories of soil consolidation and groundwater motion, except that (6.34) includes an advected time derivative which accounts for the fact that pressure diffusion occurs in debris that may move at significant rates. Equation (6.34) also includes a forcing term that accounts for evolution of the mean total stress  $\bar{T}$  and the hydrostatic component of pore pressure, quantities that change as debris-flow geometry changes. Finally, the equation contains a group of parameters ( $k/\alpha\mu$ ) that plays the role of a pore-pressure diffusivity or consolidation coefficient. Values of these parameters may, of course, evolve as debris-flow composition and bulk density evolve.

Savage and Iverson (2003) showed how (6.34) may be solved in conjunction with debris-flow dynamics equations for cases in which debris-flow motion is 1-D, excess pore pressure diffuses only normal to the bed, and pore-pressure diffusivity is a simple function of position within the flow. Denlinger and Iverson (2001) computationally solved an equation similar to (6.34), but lacking the forcing term, in conjunction with multidimensional debris-flow equations. However, completely general models that couple 3-D pore-pressure diffusion to porosity changes caused by debris-flow motion remain to be developed. Such models require consideration of the coupling between debris agitation and porosity change, perhaps through use of the “granular temperature” concept commonly used in grain-flow dynamics (e.g., Goldhirsh, 2003).

Despite the current lack of a complete model, the most important implications of pore-fluid pressures in debris flows are well established on the basis of both theory and experiments: pore pressure co-evolves with debris-flow deformation; significant pore-pressure changes can result from small changes in debris porosity; and pore-pressure changes imply commensurate changes in intergranular effective stress, which plays an important role in debris-flow mechanics owing to its influence on intergranular friction (Iverson, 1997, 2003a; Major and Iverson, 1999; Savage and Iverson, 2003).

### 6.4.3 Stress due to interactions of solid grains

Field observations and laboratory experiments indicate that contacts of solid grains against the bed and one another transfer much momentum, dissipate much energy, and therefore produce much of the stress during debris-flow motion (Iverson, 2003a). Grains can interact with the bed and one another through both enduring contacts (i.e., frictional sliding, rolling, and locking) and brief inelastic collisions. A wealth of experimental and theoretical evidence indicates that both types of interaction tend to produce intergranular shear stresses directly proportional to intergranular normal

stresses, as summarized by the Coulomb equation (e.g., Bagnold, 1954; Hungr and Morgenstern, 1984; Savage and Sayed, 1984). Therefore, estimation of intergranular shear stresses in depth-averaged debris-flow models can be based on (6.15), which provides a basis for estimating intergranular normal stress.

Coulomb (1776) proposed his well-known equation describing bulk stresses in failing masses of grains through analogy with frictional behaviour of discrete solid bodies in contact. The Coulomb equation:

$$\tau_{shear} = \sigma_{norm} \tan \varphi \quad (6.35)$$

has an apparent simplicity that belies its subtle (and sometimes complicated) implications. The equation states that the bulk intergranular shear stress  $\tau_{shear}$  on a plane of shearing is directly proportional to the bulk intergranular normal stress  $\sigma_{norm}$  acting on the same plane, irrespective of the area of grain contacts, rate of shearing, and magnitudes of stress components not acting on the plane of shearing. The proportionality constant is specified by the tangent of the friction angle  $\varphi$ .

By measuring and calculating stresses produced by collisions in a shearing mixture of neutrally buoyant spherical grains, Bagnold (1954) provided the first evidence that a Coulomb proportionality applies even in rapid, collisional grain flows. Subsequent analyses and experiments with diverse materials have generally supported Bagnold's findings and lent credibility to the Coulomb proportionality (e.g., Brown and Richards, 1970; Savage and Sayed, 1984; Hunt et al., 2002).

The Coulomb equation (6.35) may be generalized by replacing  $\sigma_{norm}$  with the intergranular effective normal stress  $\sigma_e$ , defined as  $\sigma_e = \sigma_{norm} - p$ , and by adding a cohesive strength component  $c$ . These generalizations produce the Coulomb–Terzaghi equation typically used to describe stresses during shear failure of rocks and soils (e.g., Terzaghi, 1936; Lambe and Whitman, 1979):

$$\tau_{shear} = (\sigma_{norm} - p) \tan \varphi + c \quad (6.36)$$

For granular materials subject to large deformations (as in debris flows) cohesive forces are generally negligible, and (6.36) reduces to  $\tau_{shear} = (\sigma_{norm} - p) \tan \varphi$ . Importantly, intergranular stresses are coupled to the solid-fluid interaction stresses described in the previous section through inclusion of  $p$  in (6.36).

Equation (6.36) with  $c = 0$  provides information about the state of intergranular stress in shearing debris, but does not constitute a rheological model in the usual sense, because it implies no one-to-one correspondence between stress and deformation or deformation rate. Moreover, (6.36) is a 1-D equation, and generalizing the equation to 3-D results in a complicated mathematical formulation (e.g., Desai and Siriwardane, 1984). Coulomb stress states in a 3-D medium can be represented relatively simply, however, by depicting them geometrically in a 3-D stress space in which Cartesian axes denote principal stresses (Figure 6.4). In this depiction, Coulomb stress states lie on the surface of an irregular hexagonal cone, but these states cannot be determined without some independent knowledge or concurrent calculation of deformation (e.g., Denlinger and Iverson, 2004). In this sense, the Coulomb stress model shares a property with traditional rheological models (e.g.,

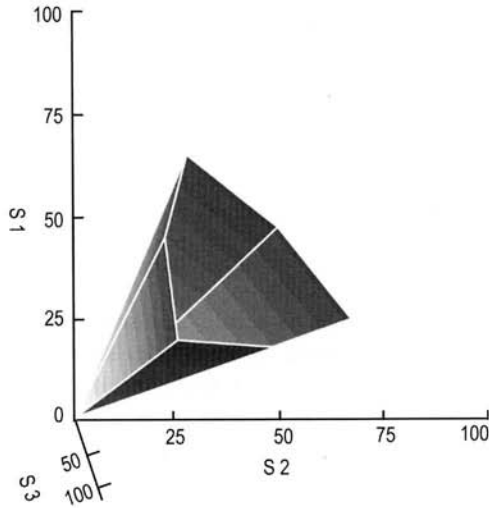


**Figure 6.4.** A Coulomb yield surface in 3-D stress space. In this space the coordinate axes represent principal stresses, but the relative magnitudes of the three principal stresses  $S_1$ ,  $S_2$ , and  $S_3$  are unspecified. See Denlinger and Iverson (2004) for further details.

viscosity, elasticity): calculation of multidimensional states of stress cannot be accomplished without calculation of deformation.

In cases where debris-flow thickness varies only gradually, however, the 1-D form of the Coulomb–Terzaghi equation (6.36) suffices to estimate basal intergranular shear stresses that resist debris-flow motion. In such cases the total stress normal to the bed can be estimated from the apparent weight of the superincumbent debris, and lateral stresses are assumed to have negligible influence on the basal shear stress. With reference to Figure 6.5, the apparent weight of a moving column of debris of constant density  $\rho$ , mean vertical height  $h$ , and horizontal planimetric area  $\Delta x \Delta y$  is  $\rho g' h \Delta x \Delta y$ , where  $g'$  is defined as in (6.16). Normal to the bed the component of apparent weight is  $\rho g' h \Delta x \Delta y \cos \theta$ , where  $\theta$  is the angle between the bed and a horizontal reference surface. The basal traction (defined as force per unit of bed area) due to this component of apparent weight is  $\rho g' h \cos^2 \theta$ . Therefore, according to (6.36), the basal Coulomb shear resistance acting parallel to the base of the debris column is approximately:

$$\tau_{shear}(b) = (\rho g' h \cos^2 \theta - p_{bed}) \tan \varphi_{bed} \quad (6.37)$$

where  $\varphi_{bed}$  denotes a friction angle appropriate for the grain–bed interface and  $p_{bed}$  is the pore-fluid pressure at this interface. For simple Coulomb sliding parallel to the bed, the basal resistance equation (6.37) takes the place of the collection of basal stress terms that appear in (6.18),  $-\tau_{zx}(b) + \tau_{xx}(b)[\partial b / \partial x] + \tau_{yx}(b)[\partial b / \partial y]$ . Moreover, (6.37) provides a first (or “lowest order” in  $H/L$ ) approximation of resistance to debris-flow motion even in more complicated cases (cf. Iverson and Denlinger, 2001).

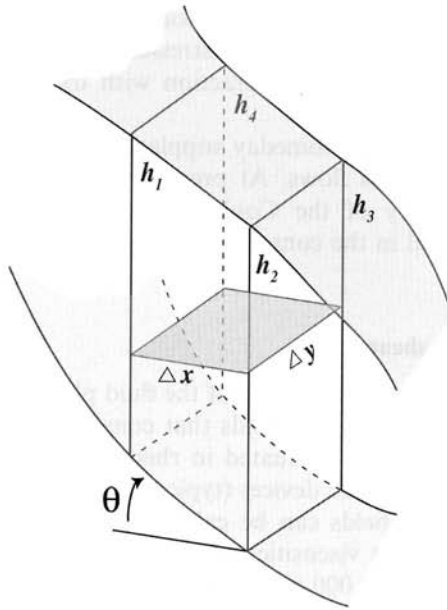


**Figure 6.5.** Geometry used to calculate the basal normal traction due to the apparent weight of a vertical column of debris with mean height  $h = (h_1 + h_2 + h_3 + h_4)/4$ . The apparent weight depends on the total vertical acceleration  $g'$  defined in (6.16).

Typical values of basal Coulomb shear stresses in debris flows may be estimated by using (6.37) in conjunction with typical parameter values such as  $h = 1\text{ m}$ ,  $\rho = 2,000\text{ kg/m}^3$ ,  $\varphi_{bed} = 30^\circ$ , and  $\theta = 5^\circ$ . With these values and  $p_{bed} = 0$ , (6.37) indicates a basal shear stress of roughly 10,000 Pa. Of course, this Coulomb shear stress will be reduced as  $p_{bed}$  increases, and will be zero in the extreme case where  $p_{bed}$  balances the total basal normal stress.

Additional Coulomb stress components that appear in (6.18) can be estimated with varying degrees of sophistication, although all such estimations require analyses that are too involved to be presented in detail here. The simplest approach entails use of lateral earth-pressure coefficients similar to those used in quasistatic soil mechanics (e.g., Lambe and Whitman, 1979). In this case depth-averaged lateral stresses such as  $\bar{\tau}_{xx}$  are related to the vertical stress  $\bar{\tau}_{zz}$  through a simple proportionality:

$$\bar{\tau}_{xx} = k_{act/pass} \bar{\tau}_{zz} \tag{6.38}$$

Values of the lateral pressure coefficient  $k_{act/pass}$  are computed by assuming Coulomb limiting equilibrium in a granular slab deforming uniformly in compression or extension (Savage and Hutter, 1989; Iverson and Denlinger, 2001).

A more accurate approach estimates all components of Coulomb stresses acting on vertical planes by using deformation kinematics to infer the location of principal stresses on the Coulomb cone of Figure 6.4 (Denlinger and Iverson, 2004). Then standard mathematical rules for tensor transformations can be employed together

with (6.15) and (6.18) to obtain all stress components. This approach may be necessary to accurately resolve Coulomb stresses where debris-flow thicknesses change abruptly as a result of flow interaction with irregular terrain (Iverson et al., 2004).

More elaborate models may someday supplant the simple Coulomb model of intergranular stresses in debris flows. At present, however, no data convincingly demonstrate the inadequacy of the Coulomb model, and as noted above, the model is particularly useful in the context of depth-averaged flow computation.

#### 6.4.4 Stress due to fluid shear

Stress also results from shear deformation of the fluid phase in debris flows. Magnitudes of shear stresses in debris-flow fluids that consist of water plus silt and clay carried in suspension have been evaluated in rheometric tests. Such tests approximate steady, uniform, 1-D flow in devices (typically rotational rheometers) in which the stress and deformation fields can be calculated exactly or measured directly. Rheometric tests indicate that viscosities of fine-grained slurries range from about 0.1 to 50 Pa-s (about 100 to 50,000 times greater than the viscosity of pure water), depending on the sediment concentration (cf. Hunt et al., 2002). Given that shear rates in debris flows are typically of the order of  $10 \text{ s}^{-1}$ , this range of viscosities implies the existence of viscous shear stresses no larger than about 500 Pa.

Rheometric measurements of muddy debris-flow slurries also reveal the existence of finite shear strengths, which contribute to stress by resisting deformation. Strengths of mud slurries typically range from about 10–400 Pa (e.g., Kang and Zhang, 1980; O'Brien and Julien, 1988; Phillips and Davies, 1991; Major and Pierson, 1992; Coussot and Piau, 1995; Locat, 1997; Parsons et al., 2001). To gain some intuitive grasp of the size of these strengths, it is instructive to slide a book across a tabletop. For diverse books and tabletops, basal shear stresses that resist sliding are comparable to the strengths in fine-grained debris-flow slurries.

Although debate continues about the best mathematical model for representing fluid shear stresses in debris-flow mixtures, the mechanical effects described above can be represented by a simple Bingham model. The 1-D form of this model can be expressed as:

$$\tau_{shear} = s_f + \mu \frac{dv_x}{dz} \quad (6.39)$$

where  $s_f$  is the fluid (slurry) shear strength and  $dv_x/dz$  is the 1-D shear deformation rate. Iverson (1985) showed how (6.39) and related rheological equations may be generalized to three space dimensions.

The basal shear stress implied by (6.39) can be expressed as a function of the depth-averaged debris-flow velocity  $\bar{v}_x$  and flow thickness  $h$  by assuming the shear stress results only from the weight of the superincumbent debris ( $\tau_{shear} = \rho g^l (\eta - z) \sin \theta \cos \theta$ , analogous to the assumption used to obtain the basal Coulomb shear stress equation (6.37)). Then integration of (6.39) from  $z = 0$  to

$z = h$  shows that the basal resistance due to fluid shear can be expressed as (cf. Bird et al., 1960, pp. 37–40):

$$\tau_{shear}(b) = s_f + 3\mu\bar{v}_x/h \quad (6.40)$$

It is useful to compare the magnitude of this fluid basal shear stress with that of the Coulomb basal shear stress described by (6.37) for a typical debris flow with bulk density  $\rho = 2,000 \text{ kg/m}^3$ , thickness  $h = 1 \text{ m}$ , and depth-averaged velocity  $\bar{v}_x = 10 \text{ m/s}$  descending a planar surface with slope  $\theta = 5^\circ$ . If the fluid slurry has typical properties  $s_f = 100 \text{ Pa}$  and  $\mu = 10 \text{ Pa-s}$ , the basal shear stress described by (6.40) then has a value of 500 Pa. In contrast, if the basal friction angle of the granular debris has a typical value  $\varphi_{bed} = 30^\circ$  and the basal pore pressure has a value  $p_{bed} = 0$ , the Coulomb basal shear stress described by (6.37) has a value of roughly 10 kPa, 20 times larger than the fluid stress. This stress ratio is reduced to 1 : 1 if the basal pore pressure nearly liquefies the mixture by balancing 95% of the total basal normal stress. In such instances fluid resistance to shear is comparable to the Coulomb shear resistance.

The foregoing discussion intentionally omits any mention of fluid turbulence. Although turbulent fluid flow might occur in debris flows, turbulence is suppressed by the presence of high concentrations of solid grains (Koch and Hill, 2001). Indeed, a crucial difference exists between fluid turbulence and the generally agitated state commonly evident in debris flows. Agitation associated with bobbing and jostling of grains in debris flows indicates the presence of disorganized kinetic energy, commonly called “granular temperature” by analogy with thermodynamic temperature in the kinetic theory of molecular gases (e.g., Haff, 1983; Iverson, 1997; Goldhirsch, 2003). Granular temperature can exist in the absence of any fluid or fluid turbulence, and it involves energy dissipation so intense that it hinders development of coherent vorticity structures like those associated with eddies in turbulent fluid flow. Further research is needed to understand the relationships between granular temperature and small-scale turbulent fluctuations of intergranular fluid in debris-flow mixtures. At present, however, inclusion of such relationships in debris-flow models would entail almost pure conjecture (cf. Koch and Hill, 2001).

#### 6.4.5 Lumped rheology and calibrated resistance formulas

As an alternative to separating the stress contributions of solid and fluid constituents and their interactions, many investigators use lumped-rheology models or calibrated resistance formulas to represent the effects of stresses throughout debris flows. In the lumped-rheology approach, debris is treated as a single-phase continuum, and the stress in (6.4a, b) is specified explicitly as a function of debris deformation or deformation rate (e.g., Iverson, 1985; Chen, 1988). Although the mathematical simplicity of this approach is appealing, the approach cannot represent evolution of stress-generation processes. Lumped-rheology equations assume that stress-generation processes remain essentially constant in space and time, whereas field observations and experimental data indicate that dominant stress-generation processes differ in the coarse granular surge fronts and nearly liquefied interiors that develop in debris flows (Iverson, 2003a).

A related factor limiting the utility of the lumped-rheology approach is the complexity and poor reproducibility of rheological properties of debris-flow materials treated as single-phase continua (Phillips and Davies, 1991; Major and Pierson, 1992). No standard devices or established protocols exist for measuring rheologies of mixtures consisting of both muddy slurry and coarse granular debris that may include gravel, cobbles, and boulders. (On the other hand, the distinct solid and fluid constituents of debris flows have mechanical properties that are clearly defined and readily measured in standard tests. The most important solid–fluid coupling parameter, the mixture permeability  $k$ , is also readily measured (Major et al., 1997).) Therefore, the relative simplicity of the lumped-rheology approach is largely illusory. Lumping rheological effects into a single equation can simplify mathematical and computational tasks, but it complicates the task of measuring relevant parameters.

Measurement difficulties can be circumvented by using calibrated resistance formulas rather than explicit rheological equations to represent the net effect of stresses in debris flows. Calibrated resistance formulas often can provide good agreement between model results and field observations, because values or even the functional forms of resistance terms can be adjusted with the explicit aim of achieving good fits. However, the appeal of good fits must be weighed against loss of the ability to perform conclusive hypothesis tests. From a scientific perspective, a mechanical model represents a hypothesis cast in precise mathematical form, but the hypothesis can be tested only if it makes unequivocal predictions. If a mechanical model is calibrated to fit data rather than tested against data, no unequivocal predictions are made, and it becomes difficult to distinguish whether good model performance reflects inherent model accuracy or merely model adaptability that is accommodated by calibration (Iverson, 2003b).

The resistance-formula approach generally focuses on adjustment of the basal shear stress (i.e.,  $\tau_{zx}(b)$  in the depth-averaged stress equation (6.18)), with the aim of fitting observations of debris-flow travel times and distances. Commonly modellers assume that  $\tau_{zx}(b)$  is some function of the depth-averaged velocity  $\bar{v}_x$  (e.g., O'Brien et al., 1993; Hungr, 1995). Any such function can be represented by a power-series expansion of the form:

$$\tau_{zx}(b) = a_0 + a_1 \bar{v}_x + a_2 \bar{v}_x^2 + \cdots + a_N \bar{v}_x^N \quad (6.41)$$

and if the coefficients  $a_0$  through  $a_N$  are freely adjustable, (6.41) can be calibrated to any desired precision (i.e., if the power series contains  $N$  terms, it can be fitted to  $N + 1$  data points exactly).

Typically debris-flow modellers restrict attention to the first three terms on the right-hand side of (6.41), and also ascribe some rheological significance to the coefficients  $a_0$ ,  $a_1$ , and  $a_2$  (e.g., O'Brien et al., 1993; Hungr, 1995). The basis for this reasoning becomes clearer if some additional factors and constants are inserted in (6.41). For example, if some appropriate factors and constants are inserted and the series expansion is truncated to two terms, (6.41) takes the form:

$$\tau_{zx}(b) = \rho g h a_0 + (3/h) a_1 \bar{v}_x \quad (6.42)$$

Here it is clear that  $a_0$  can be regarded as analogous to the basal Coulomb friction coefficient  $\tan \varphi_{bed}$  in (6.38) and  $a_1$  can be regarded as analogous to the viscosity coefficient  $\mu$  in (6.40). Thus, in principle it should be possible to determine applicable values of these coefficients using appropriate rheometric tests. Instead, in the calibrated-resistance approach, the values of coefficients such as  $a_0$  and  $a_1$  are adjusted to fit model results to field data. This adjustment constitutes the most fundamental distinction between lumped-rheology and calibrated-resistance approaches.

Another distinction between the mixture-theory, lumped-rheology, and calibrated-resistance approaches involves evaluation of stress components other than  $\tau_{zx}(b)$  in (6.18). Mixture theory assumes that solid and fluid constituents and their interactions can influence all stress components (Iverson, 1997; Iverson and Denlinger, 2001). The lumped-rheology approach similarly assumes that all stress components depend on rheology of a mixture idealized as a one-phase material. In contrast, the calibrated-resistance approach typically assumes that stresses such as  $\bar{\tau}_{xx}$  in (6.18) have a fixed form that is independent of the calibrated form of  $\tau_{zx}(b)$  (e.g., O'Brien et al., 1993). This dissociation of stress components impedes efforts to interpret calibrated resistance formulas rheologically.

## 6.5 SURGE DYNAMICS

A conspicuous and important trait of debris flows involves their tendency to move as a discrete surge or series of surges, with each surge typically exhibiting a coarse-grained head and finer grained, more-liquefied tail (Sharp and Nobles, 1953; Davies, 1990; Iverson, 1997; Hungr, 2000). The head-and-tail morphology results from mass and momentum conservation operating in conjunction with solid–fluid stress partitioning and grain-size segregation. Other phenomena, such as buoyancy and inertia due to ambient fluid surrounding a flow, can contribute significantly to head-and-tail surge morphology in dilute density currents and subaqueous debris flows, but are relatively unimportant in subaerial debris flows (Iverson, 2003c).

To illustrate some key aspects of surge dynamics, it is useful to consider a simplified depth-integrated momentum-conservation equation, which applies to an infinitely wide debris flow travelling in the  $x$  direction across a horizontal surface without erosion or deposition. In this case the  $y$  and  $z$  velocity components are zero (Figure 6.2), and the momentum conservation equation for the  $x$  direction reduces to:

$$\frac{\partial(h\bar{v}_x)}{\partial t} + \frac{\partial(h\bar{v}_x^2)}{\partial x} = -\frac{1}{\rho} \left[ \frac{\partial(\bar{\tau}_{xx}h)}{\partial x} - \tau_{zx}(b) \right] \quad (6.43)$$

which is obtained by combining (6.9) and (6.18) and eliminating terms that equal zero in this special case.

To facilitate interpretation of (6.43), the depth-averaged longitudinal normal stress  $\bar{\tau}_{xx}$  can be approximated as a gravity-induced stress that is proportional to the local debris thickness  $h$ , such that  $\bar{\tau}_{xx} = (1/2)\rho g h k_{act/pass}$ , where  $k_{act/pass}$  is the same proportionality coefficient as in (6.38) (cf. Savage and Hutter, 1989; Hungr,

1995; Iverson, 1997). Substituting this expression and the applicable form of (6.37) (i.e.,  $\tau_{zx}(b) = -(\rho gh - p_{bed}) \tan \varphi_{bed}$ ) into (6.43) yields a 1-D momentum equation in which physical aspects of surge dynamics are especially transparent:

$$\rho \left( \frac{\partial(h\bar{v}_x)}{\partial t} + \frac{\partial(h\bar{v}_x^2)}{\partial x} \right) = -\rho gh \left[ k_{act/pass} \frac{\partial h}{\partial x} + \left( 1 - \frac{p_{bed}}{\rho gh} \right) \tan \varphi_{bed} \right] \quad (6.44)$$

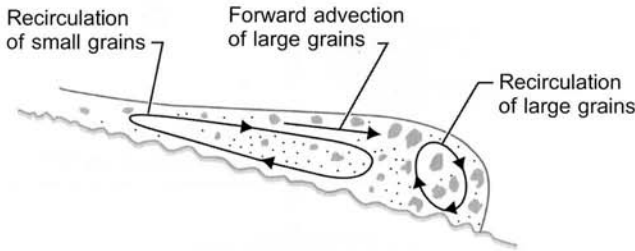
In this simplified momentum equation, longitudinal normal stresses due to the solid and fluid constituents have been lumped into a single term, but separation of these stresses is straightforward (Iverson, 1997).

All the terms in (6.44) have clear physical implications that can be couched in terms of Newton's second law of motion. The terms on the left-hand side of (6.44) express the change in momentum of the debris per unit of bed area  $\Delta x \Delta y$ , and the terms on the right-hand side express the net force on the debris per unit of bed area. These forces result from gravity and are therefore proportional to the lithostatic stress  $\rho gh$ . The term  $-\rho gh(1 - p_{bed}/\rho gh) \tan \varphi_{bed}$  expresses the basal resisting stress due to Coulomb friction, and this resistance is modulated by the basal pore pressure  $p_{bed}$ , which is generally a function of  $x$  and  $t$ . The term  $-\rho gh k_{act/pass} (\partial h/\partial x)$  expresses the variation in longitudinal normal stress due to variation in debris thickness. This term acts to drive debris forward if  $\partial h/\partial x < 0$ , as in the head of an advancing surge, whereas it acts to drive debris backward if  $\partial h/\partial x > 0$ , as in the tail of a surge. Thus, the longitudinal stress term indicates that gravitational spreading should cause surges to elongate and thereby attenuate. In contrast, observations and data show that, although debris-flow surges may elongate, attenuation of surge fronts is by no means pervasive. Instead, debris-flow surge fronts tend to grow large and steep, and secondary surge fronts tend to appear. Therefore, understanding the development and persistence of debris-flow surges and surge fronts requires delving deeper into the implications of (6.44).

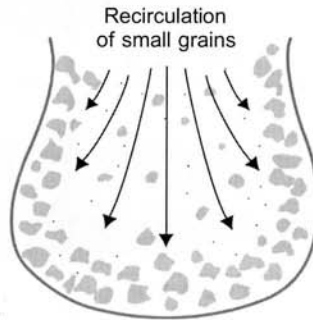
Stability analysis of an equation similar to (6.44) shows that development of small-amplitude surges can result from an interaction of inertial and gravitational effects that are present in shallow flows of any fluid-like substance, irrespective of its rheology (Forterre and Pouliquen, 2003). However, surge fronts in debris flows appear to grow to large amplitudes as a consequence of non-uniform frictional resistance that results from grain-size segregation and pore-pressure diffusion (cf. Iverson, 1997; Savage and Iverson, 2003). In (6.44), non-uniform frictional resistance is represented by a non-uniform distribution of  $-\rho gh(1 - p_{bed}/\rho gh) \tan \varphi_{bed}$ , which results mostly from variation in basal pore-fluid pressure  $p_{bed}$ . Recall from (6.34) that variation of pore-fluid pressure about an equilibrium (hydrostatic) distribution obeys a diffusion equation, and that the diffusivity  $k/\alpha\mu$  includes the permeability  $k$ , which can vary by many orders of magnitude as a consequence of variations in grain-size distributions (Iverson, 1997; Major et al., 1997). Thus, grain-size segregation in debris flows can result in great variations in dissipation of excess (non-equilibrium) pore-fluid pressure, which causes great variation in frictional resistance.

Figure 6.6 depicts schematically the means by which grain-size segregation in debris flows appears to develop and persist. As a consequence of grain-size

## A. Longitudinal cross-section view



## B. Planimetric view



**Figure 6.6.** Schematic of grain trajectories and resulting grain-size segregation in a debris-flow surge.

segregation, debris-flow surges typically have steep, coarse-grained, high-resistance heads with little excess pore-fluid pressure and relatively fine-grained, low-resistance, tapering surge tails nearly liquefied by high pore-fluid pressure (Figure 6.7). The liquefied tail tends to push against the high-friction head, which can act somewhat like a moving dam. Thus, a disparity in frictional resistance between the surge head and tail can amplify the surge waveform despite the tendency for the term  $-\rho g h k_{act/pass}(\partial h/\partial x)$  in (6.44) to attenuate the surge (Savage and Iverson, 2003).

The important role of grain-size segregation in growth of debris-flow surges is indicative of an emergent phenomenon. (“Emergent” is a term commonly used in non-linear dynamics to describe phenomena or structures that arise from dynamical feedbacks rather than from physical properties that can be specified a priori.) Indeed, any a priori specification of debris-flow rheology or flow resistance disregards a fundamental fact of debris-flow mechanics: the form of the chief macroscopic flow structure (i.e., a blunt, large-amplitude surge head followed by a tapering, more dilute tail) is contingent on a non-uniform distribution of flow resistance that evolves as a *consequence* of flow dynamics. Future progress in debris-flow mechanics may therefore depend on the degree to which grain-size segregation processes and the consequent emergence and persistence of surges can be successfully represented in continuum models.

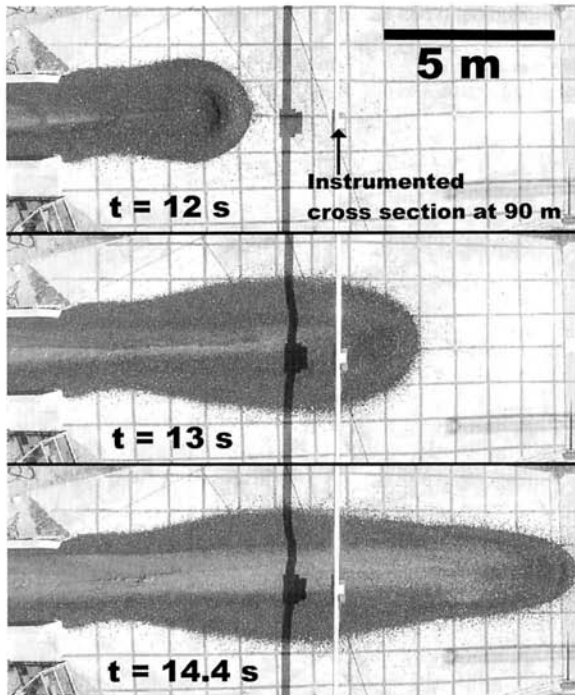


**Figure 6.7.** Aerial photographs of an experimental  $\sim 10\text{ m}^3$  debris flow discharging from the mouth of the USGS debris-flow flume. Grain-size segregation produced a surge front composed almost entirely of gravel (dark toned) and a surge tail composed of liquefied mud (light toned). Time stamps of photo frames are referenced to  $t = 0$  when the debris flow was released from a headgate 82.5 m upslope from the flume mouth. Iverson (2003a) provides further details and data on this experiment.

## 6.6 CONCLUDING REMARKS

Continuum mechanical models of debris flows are founded partly on well-established physical laws and mathematical rules, and partly on empirical and theoretical inferences about stresses that are responsible for energy dissipation. Therefore, a primary objective in mechanistic debris-flow modelling is to honor physical laws and mathematical rules as faithfully as possible, and a second objective is to link representation of stresses to data and theory in a manner that is direct and transparent.

Mechanical models of debris flows can have value as both hazard-assessment tools and precise conceptual frameworks. The conceptual value depends largely on the degree to which models link debris-flow behavior to universal scientific principles, such as conservation of momentum and mass, and to replicable experimental data. Models with weak linkages to replicable data and universal principles have limited conceptual value but may offer useful methodology for practical hazard assessment in some circumstances.

Clear tests of the predictive power of mechanistic models can be achieved only in controlled experiments in which all parameter values and boundary conditions are independently constrained. On the other hand, natural debris flows typically have indeterminate parameter values and unconstrained initial and boundary conditions, which preclude decisive model tests. As a consequence, models commonly are calibrated by adjusting stress or resistance terms to fit the observed behaviour of natural debris flows. The differences between model testing using experimental data and model calibration using field observations can have a synergistic effect, however. The two procedures can be used together to reveal model weaknesses and thereby lead to model improvements.

Predictions of debris-flow models should be regarded with ample skepticism by both model developers and model users. Scientific interpretations derived from model output are only as valid as the assumptions used in model formulation. Model developers should, therefore, make painstaking efforts to thoroughly document all physical, mathematical, and computational aspects of their models, as well as the sources and reliability of data that serve as model inputs. Model users should demand this thorough documentation and should make their own painstaking efforts to understand model limitations. Through such combined efforts of model developers and model users, mechanistic models of debris flows can be expected to improve.

## 6.7 ACKNOWLEDGEMENTS

I thank James Vallance, Joseph Walder, and the editors for their constructive criticism of a preliminary draft of this chapter. Dr. Vallance provided a draft version of Figure 6.6.

## 6.8 REFERENCES

- Abramowitz, M. and Stegun, I.A. (eds) (1964) *Handbook of Mathematical Functions with Formulas, Graphs, and Mathematical Tables* (1046 pp.). US Department of Commerce, National Bureau of Standards, Washington, DC.
- Asmar, B.N., Langston, P.A., and Ergenzinger, P. (2003) The potential of the discrete element method to simulate debris flow. In: D. Rickenmann and C-L. Chen (eds), *Debris-flow Hazards Mitigation: Mechanics Prediction and Assessment* (Vol. 1, pp. 435–445). Millpress, Rotterdam.
- Bagnold, R.A. (1954) Experiments on a gravity-free dispersion of large solid spheres in a Newtonian fluid under shear, *Proceedings of the Royal Society of London, Ser. A*, **225**, 49–63.
- Bear, J. (1972) *Dynamics of Fluids in Porous Media* (764 pp.). Dover, New York.
- Bird, R.B., Stewart, W.E., and Lightfoot, E.N. (1960) *Transport Phenomena* (780 pp.). John Wiley & Sons, New York.
- Brown, R.L. and Richards, J.C. (1970) *Principles of Powder Mechanics* (221 pp.). Pergamon Press, Oxford, UK.

- Campbell, C.S., Cleary, P.W., and Hopkins, M.A. (1995) Large-scale landslide simulations: Global deformation, velocities and basal friction. *Journal of Geophysical Research B*, **100**, 8267–8283.
- Chen, C-L. (1988) Generalized viscoplastic modeling of debris flow. *Journal of Hydraulic Engineering*, **114**, 237–258.
- Chen, C-L. (ed.) (1997) *Debris-flow Hazards Mitigation: Mechanics, Prediction, and Assessment* (817 pp.). American Society of Civil Engineers, New York.
- Coulomb, C.A. (1776) Sur une application des règles de maxima & minima à quelques problèmes de statique, relatifs à l'architecture. In: *Mémoires de Mathématique et de Physique, Presented at the Royal Academy of Sciences, 1773* (pp. 343–384). Imp. R. Acad. Sci., Paris.
- Coussot, P. and Piau, J-M. (1995) A large-scale field coaxial cylinder rheometer for the study of the rheology of natural coarse suspensions. *Journal of Rheology*, **39**, 105–124.
- Davies, T.R.H. (1990) Debris-flow surges: Experimental simulation. *Journal of Hydrology (N.Z.)*, **29**, 18–46.
- Denlinger, R.P. and Iverson, R.M. (2001) Flow of variably fluidized granular masses across three-dimensional terrain: 2. Numerical predictions and experimental tests. *Journal of Geophysical Research B*, **106**, 553–566.
- Denlinger, R.P. and Iverson, R.M. (2004) Granular avalanches across irregular three-dimensional terrain: 1. Theory and computation. *Journal of Geophysical Research F*, **109**, doi:10.1029/2003JF000085, 14 pp.
- Desai, C.S. and Siriwardane, H.J. (1984) *Constitutive Laws for Engineering Materials, with Emphasis on Geologic Materials* (468 pp.). Prentice Hall, Englewood Cliffs, NJ.
- Drew, D.A. and Lahey, R.T. (1993) Analytical modeling of multiphase flow. In: M.C. Roco (ed.), *Particulate Two-Phase Flow* (pp. 509–566). Butterworth-Heinemann, Boston.
- Erlichson, H. (1991) A mass-change model for the estimation of debris-flow runout, a second discussion: Conditions for the application of the rocket equation. *Journal of Geology*, **99**, 633–634.
- Forterre, Y. and Pouliquen, O. (2003) Long-surface-wave instability in dense granular flows. *Journal of Fluid Mechanics*, **486**, 21–50.
- Gidaspow, D. (1994) *Multiphase Flow and Fluidization* (467 pp.). Academic Press, Boston.
- Goldhirsh, I. (2003) Rapid granular flows. *Annual Review of Fluid Mechanics*, **35**, 267–293.
- Gray, J.M.N.T., Wieland, M., and Hutter, K. (1999) Gravity driven free surface flow of granular avalanches over complex basal topography *Proceedings of the Royal Society of London, Ser. A*, **455**, 1841–1874.
- Haff, P.K. (1983) Grain flow as a fluid-mechanical phenomenon. *Journal of Fluid Mechanics*, **134**, 401–430.
- Hungr, O. (1995) A model for the runout analysis of rapid flow slides, debris flows, and avalanches. *Canadian Geotechnical Journal*, **32**, 610–623.
- Hungr, O. (2000) Analysis of debris flow surges using the theory of uniformly progressive flow, *Earth Surface Processes and Landforms* **25**, 483–495.
- Hungr, O. and Morgenstern, N.R. (1984) Experiments on the flow behaviour of granular materials at high velocity in an open channel. *Géotechnique*, **34**, 405–413.
- Hunt, M.L., Zenit, R., Campbell, C.S., and Brennen, C.E. (2002) Revisiting the 1954 suspension experiments of R.A. Bagnold. *Journal of Fluid Mechanics*, **452**, 1–24.
- Iverson, R.M. (1985) A constitutive equation for mass-movement behavior. *Journal of Geology*, **93**, 143–160.
- Iverson, R.M. (1997) The physics of debris flows. *Reviews of Geophysics*, **35**, 245–296.

- Iverson, R.M. (2003a) The debris-flow rheology myth. In: D. Rickenmann and C.L. Chen (eds), *Debris-flow Hazards Mitigation: Mechanics, Prediction, and Assessment* (Vol. 1, pp. 303–314). Millpress, Rotterdam.
- Iverson, R.M. (2003b) How should mathematical models of geomorphic processes be judged? In: P.R. Wilcock and R.M. Iverson (eds), *Prediction in Geomorphology* (Geophysical Monograph 135, pp. 83–94). American Geophysical Union, Washington, DC.
- Iverson, R.M. (2003c) Gravity-driven mass flows. In: G.V. Middleton (ed.), *Encyclopedia of Sediments and Sedimentary Rocks* (pp. 347–353). Kluwer, Dordrecht, The Netherlands.
- Iverson, R.M. and Denlinger, R.P. (2001) Flow of variably fluidized granular masses across three-dimensional terrain: 1. Coulomb mixture theory. *Journal of Geophysical Research B*, **106**, 537–552.
- Iverson, R.M. and Vallance, J.W. (2001) New views of granular mass flows. *Geology*, **29**, 115–118.
- Iverson, R.M., Reid, M.E., and LaHusen, R.G. (1997) Debris-flow mobilization from landslides. *Annual Review of Earth and Planetary Sciences*, **25**, 85–138.
- Iverson, R.M., Reid, M.E., Iverson, N.R., LaHusen, R.G., Logan, M., Mann, J.E., and Brien, D.L. (2000) Acute sensitivity of landslide rates to initial soil porosity. *Science*, **290**, 513–516.
- Iverson, R.M., Logan, M., and Denlinger, R.P. (2004) Granular avalanches across irregular three-dimensional terrain: 2. Experimental tests. *Journal of Geophysical Research F*, **109**, doi:10.1029/2003JF000084, 16 pp.
- Kang, Z. and Zhang, S. (1980) A preliminary analysis of the characteristics of debris flow. *Proceedings of the International Symposium on River Sedimentation* (pp. 225–226). Chinese Society for Hydraulic Engineering, Beijing.
- Keller, J.B. (2003) Shallow-water theory for arbitrary slopes of the bottom. *Journal of Fluid Mechanics*, **489**, 345–348.
- Koch, D.L. and Hill, R.J. (2001) Inertial effects in suspension and porous-media flows. *Annual Review of Fluid Mechanics*, **33**, 619–647.
- Lambe, T.W. and Whitman, R.V. (1979) *Soil Mechanics, SI Version* (553 pp.). John Wiley & Sons, New York.
- Locat, J. (1997) Normalized rheological behavior of fine muds and their properties in a pseudoplastic regime. In: C-L. Chen (ed.), *Debris-flow Hazards Mitigation: Mechanics, Prediction, and Assessment* (pp. 260–269). American Society of Civil Engineers, New York.
- Major, J.J. and Iverson, R.M. (1999) Debris-flow deposition: Effects of pore-fluid pressure and friction concentrated at flow margins. *Geological Society of America Bulletin*, **111**, 1424–1434.
- Major, J.J. and Pierson, T.C. (1992) Debris-flow rheology: Experimental analysis of fine-grained slurries. *Water Resources Research*, **28**, 841–857.
- Major, J.J., Iverson, R.M., McTigue, D.F., Macias, S., and Fiedorowicz, B.K. (1997) Geotechnical properties of debris-flow sediments and slurries. In: C-L. Chen (ed.), *Debris-flow Hazards Mitigation: Mechanics, Prediction, and Assessment* (pp. 249–259). American Society of Civil Engineers, New York.
- Malvern, L.E. (1969) *Introduction to the Mechanics of a Continuous Medium* (713 pp.). Prentice Hall, Englewood Cliffs, NJ.
- O'Brien, J.S. and Julien, P.Y. (1988) Laboratory analysis of mudflow properties. *Journal of Hydraulic Engineering*, **114**, 877–887.
- O'Brien, J.S., Julien, P.Y., and Fullerton, W.T. (1993) Two-dimensional water flood and mudflow simulation. *Journal of Hydraulic Engineering*, **119**, 244–261.

- Parsons, J.D., Whipple, K.X., and Simioni, A. (2001) Experimental study of the grain-flow, fluid-mud transition in debris flows. *Journal of Geology*, **109**, 427–447.
- Passman, S.L. and McTigue, D.F. (1986) A new approach to the effective stress principle. In: S.K. Saxena (ed.), *Compressibility Phenomena in Subsidence* (pp. 79–91). Engineering Foundation, New York.
- Phillips, C.J. and Davies, T.R.H. (1991) Determining rheological parameters of debris flow material. *Geomorphology*, **4**, 101–110.
- Rickenmann, D. and Chen, C-L. (eds) (2003) *Debris-flow Hazards Mitigation: Mechanics, Prediction, and Assessment* (1335 pp.). Millpress, Rotterdam.
- Savage, S.B. and Hutter, K. (1989) The motion of a finite mass of granular material down a rough incline. *Journal of Fluid Mechanics*, **199**, 177–215.
- Savage, S.B. and Hutter, K. (1991) The dynamics of avalanches of granular materials from initiation to runout Part I: Analysis. *Acta Mechanica*, **86**, 201–223.
- Savage, S.B. and Iverson, R.M. (2003) Surge dynamics coupled to pore-pressure evolution in debris flows. In: D. Rickenmann and C-L. Chen (eds), *Debris-flow Hazards Mitigation: Mechanics, Prediction, and Assessment* (Vol. 1, pp. 503–514). Millpress, Rotterdam.
- Savage, S.B. and Sayed, M. (1984) Stresses developed in dry cohesionless granular materials sheared in an annular shear cell. *Journal of Fluid Mechanics*, **142**, 391–430.
- Sharp, R.P. and Nobles, L.H. (1953) Mudflow of 1941 at Wrightwood, southern California. *Geological Society of America Bulletin*, **64**, 547–560.
- Terzaghi, K. (1936) The shearing resistance of saturated soils. *Proceedings of the 1st International Conference on Soil Mechanics* (Vol. 1, pp. 54–56).
- Vanoni, V.A. (ed.) (1975) *Sedimentation Engineering* (745 pp.). American Society of Civil Engineers, New York.
- Vreugdenhil, C.B. (1994) *Numerical Methods for Shallow-water Flow* (261 pp.). Kluwer Academic, Dordrecht, The Netherlands.
- Walton, O.R. (1993) Numerical simulation of inelastic, frictional particle–particle interactions. In: M.C. Roco (ed.), *Particulate Two-Phase Flow* (pp. 884–911). Butterworth-Heinemann, Boston.
- Wieczorek, G.F. and Naeser, N.D. (eds) (2000) *Debris-flow Hazards Mitigation: Mechanics, Prediction, and Assessment* (608 pp.). A.A. Balkema, Rotterdam.
- Yamagishi, M., Mizuyama, T., Satofuka, Y., and Mizuno, H. (2003) Behavior of big boulders in debris flow containing sand and gravel. In: D. Rickenmann, and C-L. Chen (eds), *Debris-flow Hazards Mitigation: Mechanics, Prediction, and Assessment* (Vol. 1, pp. 411–420). Millpress, Rotterdam.